Available online at www.sciencedirect.com
ScienceDirect
Journal of the European Ceramic Society 27 (2007) 781–789
www.elsevier.com/locate/jeurceramsoc

Microstructure and mechanical properties of silicon carbide pressureless sintered with oxide additives

Agnieszka Gubernat *, Ludosław Stobierski, Paweł Łabaj

AGH University of Science and Technology, Faculty of Materials Science and Ceramics, Department of Advanced Ceramics, Al. Mickiewicza 30, 30-059 Cracow, Poland

Available online 26 May 2006

Abstract

It is known that SiC powders can be densified at relatively low temperatures (1850–2000 °C) with some oxide additions. In this work the densification behavior, microstructure and mechanical properties (bending strength, fracture toughness, hardness) of SiC ceramics pressureless sintered with different additions chosen from oxide groups: $Al_2O_3 + Y_2O_3$, $Al_2O_3 + Y_2O_3 + MgO$, were investigated. It was found that oxide additives facilitate densification of sinters and significantly improve mechanical properties of SiC ceramics. The best activating oxide additions have been identified.

Keywords: Silicon carbide; Mechanical properties

1. Introduction

The two elements forming solid SiC structure co-exist in the state of sp^3 orbital hybridization, thus forming four localized bonds of tetrahedral symmetry. However, slight difference of electronegativity of components leads to partial polarization of molecular orbitals, which introduces some ionic component to chemical bond.[1] Valuable properties of silicon carbide, including very high hardness, excellent thermal, chemical and erosion resistance, are the results of the existence of this strong directional chemical bond. On the other hand strong covalent bond imposes low values of self-diffusion of carbon and silicon within SiC structure. This is the principal reason for low sinterability of pure SiC, thus the use of sintering activators (like boron + carbon or MeO) is necessary in its sintering.

Due to introduction of small amounts of boron and carbon to SiC powder, since the early 70s of the past century[2] the technology of manufacturing of dense quasi-monophase SiC sinters has become manageable.[2] Such materials have excellent all the above mentioned properties, while the increase of their mechanical strength and fracture toughness still remains the challenge for improvement. Significant, almost 100% increase of these properties,[3–7] may be achieved using oxide additives as sintering aids (R.A. Alliegro, 1956; F.F. Lange, 1975; K. Suzuki, 1982; R.A. Cutler, 1989), originating from the following systems: SiO_2–Al_2O_3; Al_2O_3–Y_2O_3; Al_2O_3–Y_2O_3–MgO; Al_2O_3–Y_2O_3–CaO and Al_2O_3–Y_2O_3–C.

It is believed that above oxides either due to reaction with passivating silica layer coating the SiC grains, or due to reaction among themselves, form liquid phases during sintering. On one hand they activate the densification processes, and on the other they improve some material's properties. Strength increase may be explained by filling pores by glassy phase, which decreases efficiently the number of stress concentrating defects, whereas the increase in fracture toughness may be achieved by change in fracture mechanism itself.

The aim of the present work was the development of dense SiC materials with use of pressureless sintering process activation by oxide additives such as $Al_2O_3 + Y_2O_3$ and $Al_2O_3 + Y_2O_3 + MgO$ mixtures, applied in the appropriate weight ratios. Best sintered materials had phase analyses performed, also their microstructures and mechanical properties have been examined in detail, namely: Young and Kirchoff moduli, Poisson ratio, bending strength, fracture toughness, Vickers and Knoop hardness.

2. Materials preparation and testing techniques

Figs. 1 and 2 show schematically the raw materials' preparation process and the conditions of sintering applied. Following were the sintering variables: sintering temperature, soaking time

* Corresponding author. Tel.: +48 12 617 36 96; fax: +48 12 633 46 30.
E-mail address: gubernat@uci.agh.edu.pl (A. Gubernat).

0955-2219/$ – see front matter © 2006 Elsevier Ltd. All rights reserved.
doi:10.1016/j.jeurceramsoc.2006.04.009

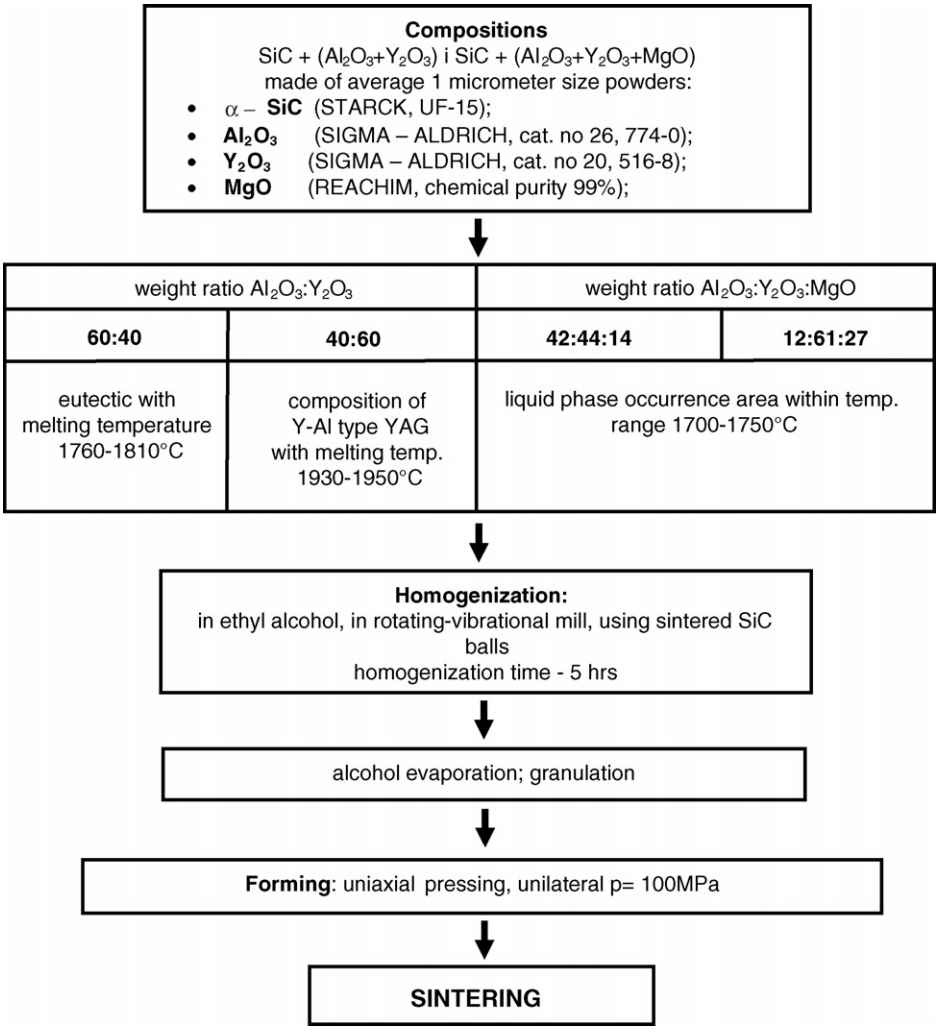

Fig. 1. The diagram of raw-materials preparation.

and application of mould powder. After sintering the apparent density (ρ_p) of all samples was measured by the Archimedes method. Materials with highest density were chosen for phase and microstructural analyses, as well as for mechanical properties testing.

The Young (E), Kirchoff (G) moduli and the Poisson ratio (ν) were determined by ultrasonic method (UZP-01; Inco Veritas). Hardness has been measured by Vickers (HV) and Knoop (HK) techniques, while fracture toughness (K_{Ic}) was determined by indentation; all tests performed on polished sections of sintered samples (Future-Tech Corp. FV-700). The three-point bending strength was measured on 40 mm × 6 mm × 4 mm rectangular bars with polished surfaces. Additionally, samples of the same dimensions were used for determination of fracture toughness (K_{Ic}) by three-point bending of notched-beam specimens method. Mechanical tests were performed using Zwick 1435 standard testing machine.

Visualization of grain boundaries was achieved by 15–20 min etching of samples in boiling 10% solution (2:1 ratio) of KOH and $K_3[Fe(CN)_6]$. Prior to etching the samples were polished using polishing clothes and disks. Microstructural observations were carried out using optical (Nikon Epiphot 300) and scanning electron (Jeol 5400) microscopes. The phase composition was determined by X-ray technique (X'Pert Pro; Philips), while elemental analysis was performed using the EDS microanalyser (Link ISIS; Oxford Instruments).

3. Results

Table 1 shows the relative density of SiC materials with varying quantities and weight proportions of activating oxides, all pressureless sintered within the temperature range 1900–2000 °C. Two sintering methods were applied: in free contact with surrounding atmosphere and in SiC mould powder. Table 2 shows the results of phase analyses obtained from X-ray diffraction studies.

Table 3 collects the results of properties testing: Young (E) and Kirchoff (G) moduli, Poisson ratio (ν), bending strength (σ_b) as well as fracture toughness (K_{Ic}) measured using two techniques: indentation and bending of notched beam. The results of hardness tests are shown in Fig. 3 for Knoop, and in Fig. 4 for Vickers technique.

Figs. 5–7 show representative microstructures of sinters activated with oxide additives having variable amount and weight

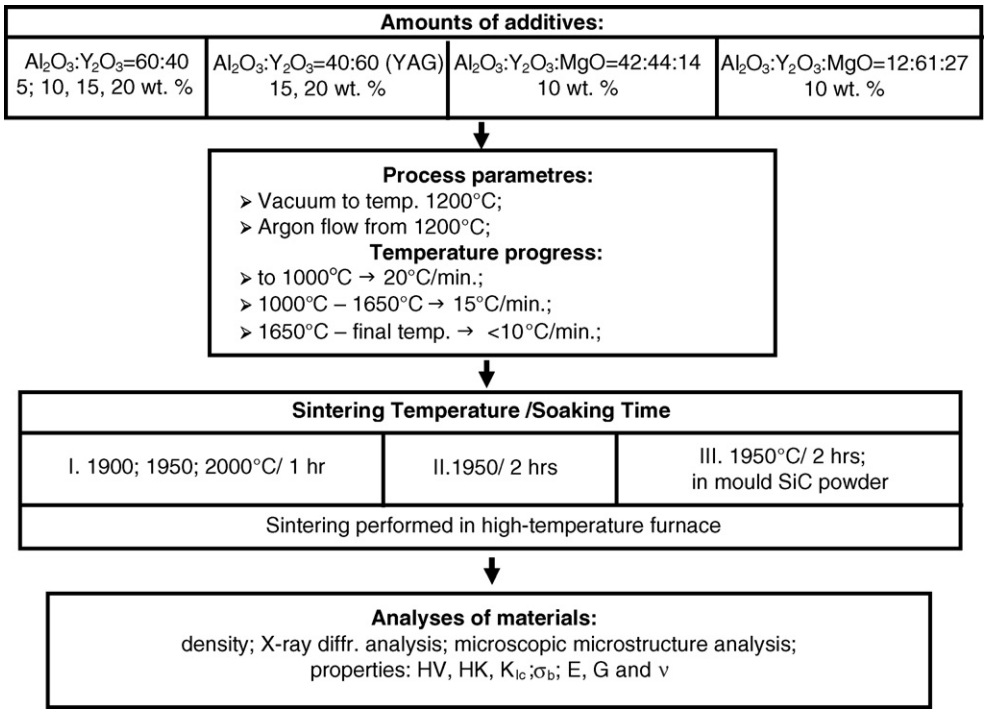

Fig. 2. The diagram of pressureless sintering process.

Table 1
The relative density of SiC materials with varying quantities and weight proportions of activating oxides

wt.% of additive	Additive composition (weight ratio)			TD (g/cm^3)	Relative density (%)				
	Al_2O_3	Y_2O_3	MgO		1900 °C, 1 h	1950 °C, 1 h	1950 °C, 2 h	1950 °C, 2 h in mould powder	2000 °C, 1 h
5	60	40	–	3.25	90 ± 4.0	94 ± 3.0	95 ± 3.5	94 ± 1.5	85 ± 2.0
10	60	40	–	3.30	94 ± 1.0	94 ± 0.5	94 ± 0.5	96 ± 0.5	84 ± 0.5
15	60	40	–	3.34	91 ± 1.5	95 ± 1.5	93 ± 0.5	95 ± 0.5	82 ± 2.0
20	60	40	–	3.39	93 ± 0.5	93 ± 2.5	92 ± 0.5	95 ± 0.5	83 ± 1.0
15	40	60	–	3.36	95 ± 0.5	91 ± 4.0	93 ± 0.5	95 ± 0.5	86 ± 1.5
20	40	60	–	3.41	94 ± 0.5	95 ± 1.0	93 ± 0.5	94 ± 0.5	81 ± 1.0
10	42	44	14	3.29	82 ± 4.0	89 ± 0.5	77 ± 3.5	96 ± 0.5	79 ± 2.0
10	12	61	27	3.29	80 ± 1.0	81 ± 3.5	81 ± 1.0	93 ± 0.5	74 ± 0,5

Table 2
The results of phase analyses obtained from X-ray diffraction studies

wt.% of additive	Additive composition (weight ratio)			XRD results
	Al_2O_3	Y_2O_3	MgO	
5	60	40	–	6H-SiC, 4H-SiC
10	60	40	–	6H-SiC, 4H-SiC, Al_2O_3, $Y_4Al_2O_9$ (YAM)
15	60	40	–	6H-SiC, 4H-SiC, Al_2O_3, $Y_3Al_5O_{12}$ (YAG)
20	60	40	–	6H-SiC, 4H-SiC, Al_2O_3, $Y_3Al_5O_{12}$ (YAG); C (graphite)
15	40	60	–	6H-SiC, 4H-SiC, $Y_3Al_5O_{12}$ (YAG)
20	40	60	–	6H-SiC, 4H-SiC, $Y_3Al_5O_{12}$ (YAG)
10	42	44	14	6H-SiC, 4H-SiC, $MgAl_2O_4$, $Y_3Al_5O_{12}$ (YAG)
10	12	61	27	6H-SiC, 4H-SiC, $MgAl_2O_4$, $Y_4Al_2O_9$ (YAM)

Table 3
The results of properties testing: Young (E) and Kirchoff (G) moduli, Poisson ratio (ν), bending strength (σ_b) as well as fracture toughness (K_{Ic}) measured using two techniques: indentation and bending of notched beam

wt.% of additive	Additive composition (weight ratio)			Three-point bending strength (MPa)	Fracture toughness (MPa m$^{0.5}$)		Young modulus (GPa)	Kirchoff modulus (GPa)	Poisson ratio
	Al_2O_3	Y_2O_3	MgO		Indentation method	Notched beam			
5	60	40	–	332.15 ± 47.96	4.92 ± 0.36	5.14 ± 0.43	298.81 ± 11.29	128.29 ± 0.24	0.17 ± 0.02
10	60	40	–	455.23 ± 56.19	5.90 ± 0.20	5.23 ± 0.70	331.48 ± 1.82	141.09 ± 0.75	0.18 ± 0.01
15	60	40	–	470.14 ± 19.69	5.66 ± 0.36	4.80 ± 0.49	307.82 ± 2.73	131.57 ± 0.34	0.17 ± 0.01
20	60	40	–	498.22 ± 49.34	5.61 ± 0.29	5.42 ± 0.50	313.46 ± 3.10	132.01 ± 0.59	0.19 ± 0.01
15	40	60	–	470.19 ± 100.54	4.87 ± 0.29	5.65 ± 0.76	340.25 ± 2.83	145.71 ± 1.14	0.17 ± 0.01
20	40	60	–	450.34 ± 60.21	5.23 ± 0.16	5.80 ± 0.19	315.41 ± 3.12	133.21 ± 0.57	0.17 ± 0.01
10	42	44	14	440.09 ± 90.45	5.24 ± 0.11	6.21 ± 0.40	341.82 ± 4.01	146.07 ± 0.36	0.17 ± 0.01
10	12	61	27	376.79 ± 61.26	4.77 ± 0.53	5.30 ± 0.77	324.84 ± 4.19	147.00 ± 0.81	0.17 ± 0.01

ratio of oxides. The results of point and line EDS analyses of precipitates observed under optical and scanning microscopes are shown in Fig. 8. Microcracks were initiated within the materials by Vickers indenter in order to define the fracture path, and pictures of such crack paths are shown in Figs. 9 and 10. The map of distribution of stresses within the material containing 15% (40% Al_2O_3 + 60% Y_2O_3) was computer generated using Pro/Mechanica software and it is shown in Fig. 11.

4. Discussion of results

The highest degree of densification, close to 95% of theoretical density, is achieved by all materials sintered in coarse-grained SiC mould powder at the temperature of 1950 °C and soaked at this temperature for 2 h. The effect of mould powder is also reflected in 40% limitation of mass loss. When sintering is carried out in unlimited contact with gas atmosphere, the mass losses for materials activated with $Al_2O_3 + Y_2O_3$ vary from 5% to 25%. The higher the activator addition, the higher the losses, whereas for group of materials activated with $Al_2O_3 + Y_2O_3 + MgO$ the mass losses vary within narrower range of 6–9%.

The results of XRD phase analysis presented in the Table 2 confirm that obtained materials are of polyphase nature. The crystalline phases present in these sinters, like: YAG—$Y_3Al_5O_{12}$, YAM—$Y_4Al_2O_9$, spinel—$MgAl_2O_4$, are most probably the phases formed by reactions among the additives. It is very likely that they are residues from liquid phases formed at given sintering conditions, or they may have been formed as a result of solid-state reactions of additives. In sinters activated with 60% Al_2O_3 + 40% Y_2O_3 in the amounts of 15% and 20%, additionally the presence of free alumina has been identified. Microscopic observations of unetched materials showed the presence of other phases' grains within the SiC matrix. As the EDS analyses confirm, these phases are rich in elements originating from oxide additives, i.e. aluminum and yttrium (Fig. 8). These are probably the precipitates identified by X-ray phase analysis (Table 2). During microspopic observations of sinters activated using Al_2O_3, Y_2O_3 and MgO oxides, the magnesium–aluminum spinel has not been identified, although its presence in these sinters was confirmed on the basis of XRD analysis. In these samples also traces of randomly distributed Mg have been found.

Microstructural observations (Fig. 6) of etched samples activated with Al_2O_3 and Y_2O_3 (weight ratio Al_2O_3:Y_2O_3 = 60:40) allow to notice that unidirectional grain growth dominates in these sinters. Only in sinters activated with 20% oxide additions the average grain size decreases and isometric smaller grains appear along with directionally growing grains. Similar microstructural pictures made of mostly small, isometric grains can be observed in oxide activated sinters with 40% Al_2O_3 + 60% Y_2O_3 (Fig. 7a) as well as in sinters activated with $Al_2O_3 + Y_2O_3 + MgO$ (Fig. 7b). In these materials also small contribution of directional or isometric larger grains can be observed (Fig. 7), which may result from non-uniformity of the initial composition. Both, directional grain growth as well as the presence of large, isometric grains, together with occur-

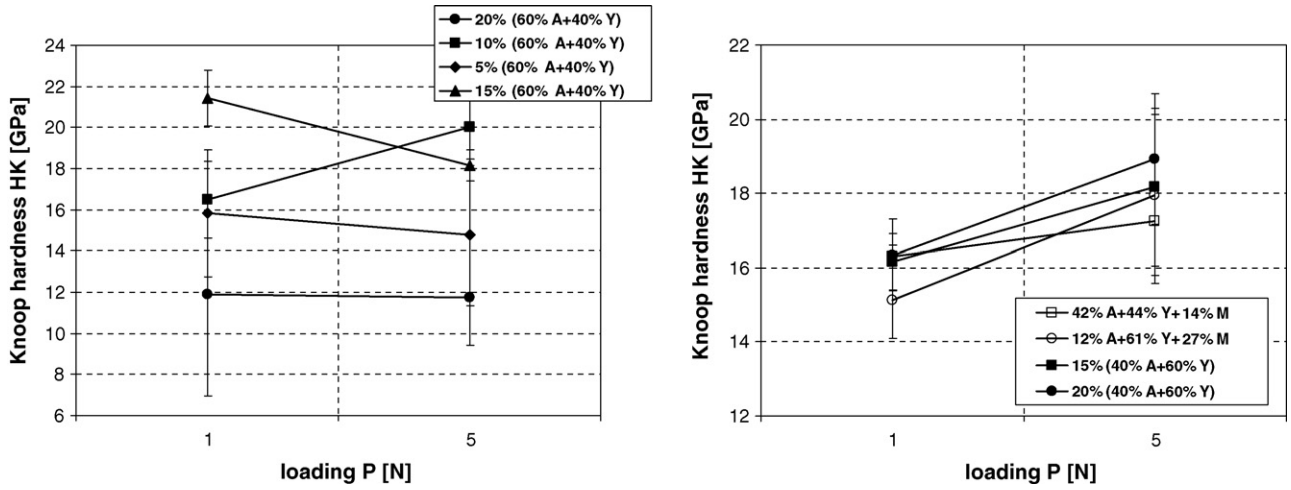

Fig. 3. Knoop hardness (on these plots: (A) Al_2O_3, (Y) Y_2O_3, and (M) MgO).

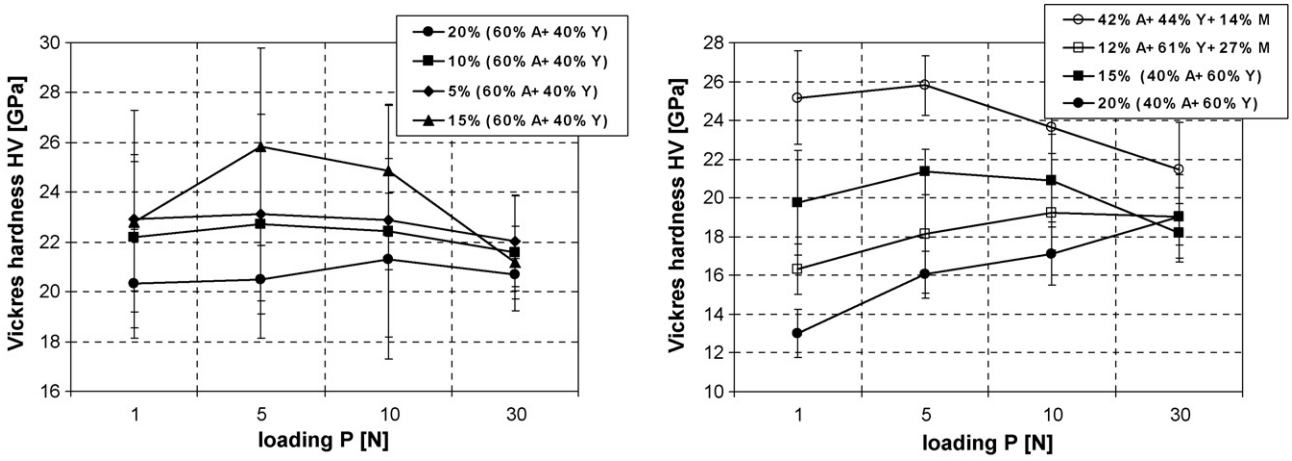

Fig. 4. Vickers hardness (same symbols as in Fig. 3).

rence of fine grains, allows to suggest the hypothesis of the presence of reactive liquid phases taking part in the densification process.

The values of Young and Kirchoff moduli and Poisson ratio shown in Table 3 remain within relatively narrow limits; Young modulus: 300–340 GPa, Kirchoff modulus: 130–150 GPa and Poisson ratio: 0.16–0.19, respectively. The relationship between Young modulus and density can be noticed, in particular for materials with oxide additions $Al_2O_3 + Y_2O_3$, of weight ratio Al_2O_3:Y_2O_3 = 60:40.

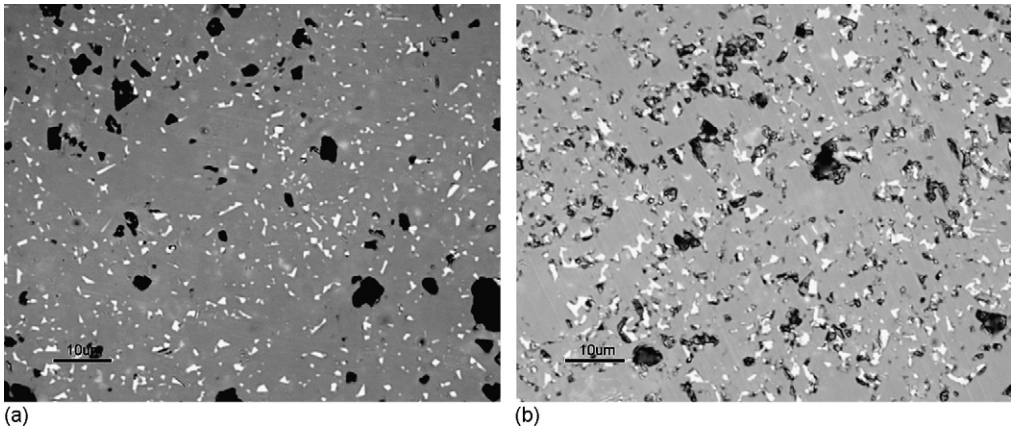

Fig. 5. Microstructures of unetched samples with visible oxide phase precipitates: (a) SiC + 5% ($60Al_2O_3 + 40Y_2O_3$) and (b) SiC + 20% ($60Al_2O_3 + 40Y_2O_3$).

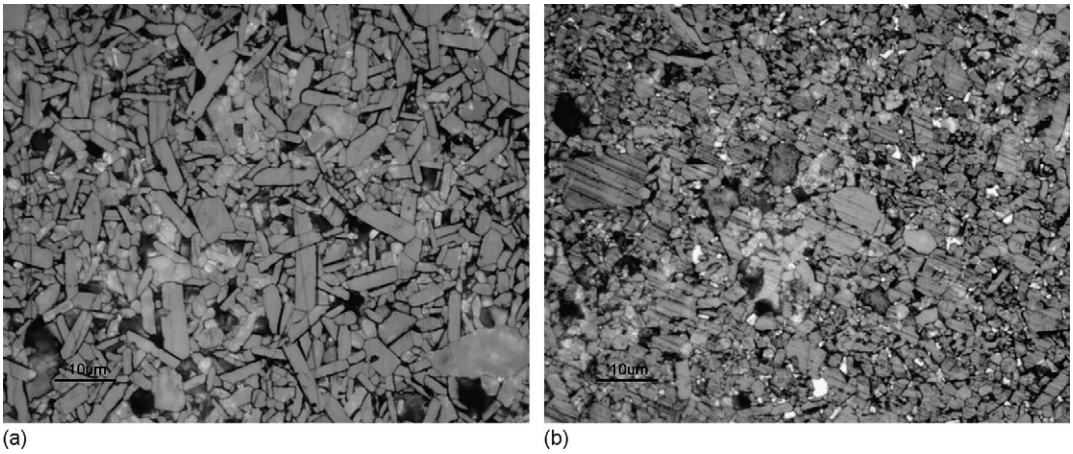

Fig. 6. Microstructures of etched samples: (a) SiC + 10% (60%Al_2O_3 + 40%Y_2O_3) and (b) SiC + 20% (60%Al_2O_3 + 40%Y_2O_3).

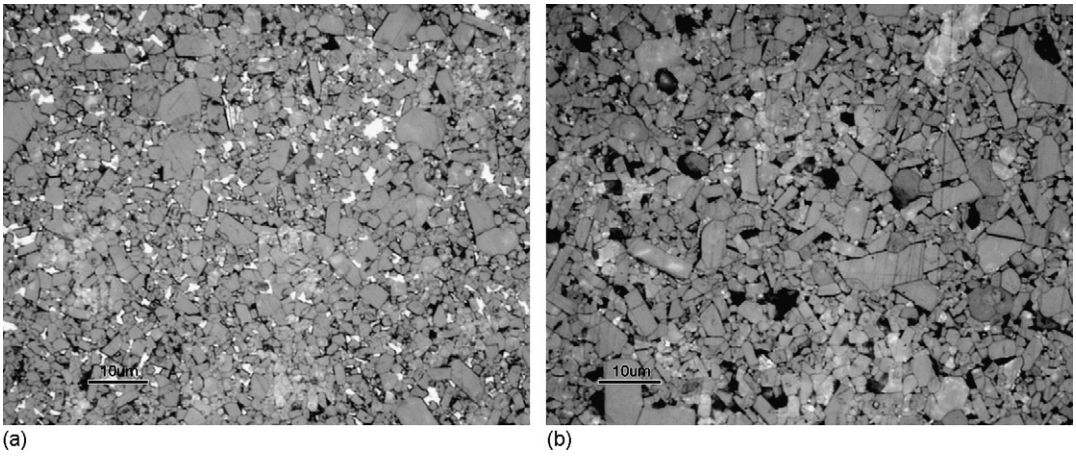

Fig. 7. Microstructures of etched samples: (a) SiC + 20% (40%Al_2O_3 + 60%Y_2O_3) and (b) SiC + 10% (42%Al_2O_3 + 44%Y_2O_3 + 14%MgO).

The Knoop hardness is lower than Vickers hardness for all examined materials and it remains within the limits ranging from 10 to 22 GPa for materials activated with 60% Al_2O_3 + 40% Y_2O_3. The Knoop hardness values within relatively close range (14–18 GPa) were achieved by materials activated with 40% Al_2O_3 + 60% Y_2O_3, and also by materials activated with Al_2O_3 + Y_2O_3 + MgO oxides.

The Vickers hardness varies significantly for three groups of materials sintered. It achieves the highest values, above 20 GPa, in the group of sinters activated with oxides 60%

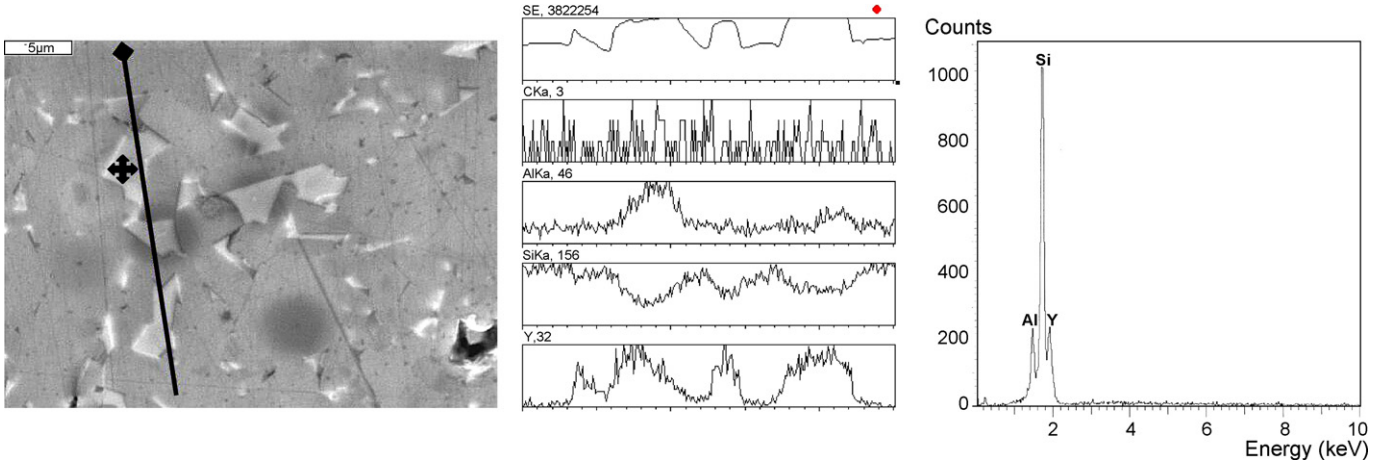

Fig. 8. The EDS line and point analyses of oxide phase precipitates.

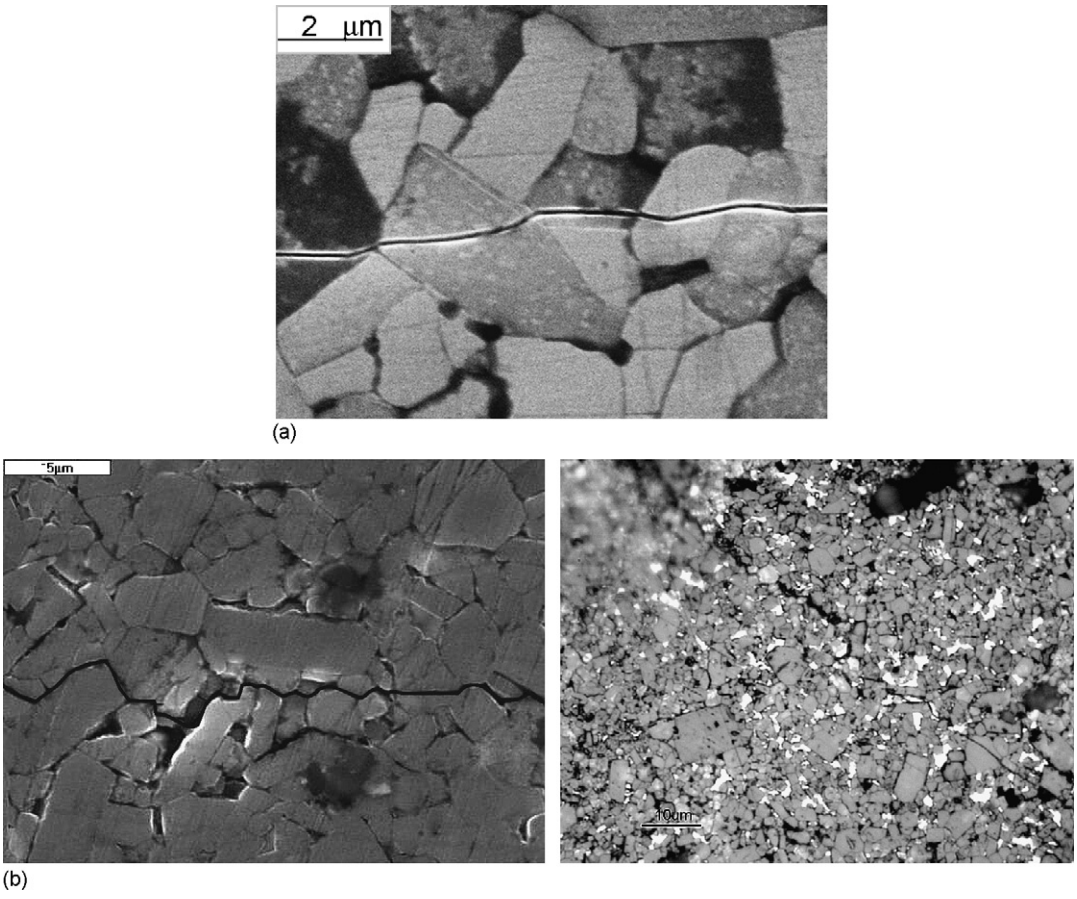

Fig. 9. Change in nature of fracture, from cross-granular (a) in monophase sinters, to intergranular (b) in oxide additive activated sinters.

$Al_2O_3 + 40\%$ Y_2O_3. In the group of materials doped with 40% $Al_2O_3 + 60\%$ Y_2O_3 oxides, high hardness values (~20 GPa) were achieved by sinters containing 15% of additives, whereas the hardness of sinters containing 20% of such oxide additives does not exceed 20 GPa. Within the group of materials activated using $Al_2O_3 + Y_2O_3 + MgO$ oxides, materials with oxide weight ratio Al_2O_3:Y_2O_3:MgO = 12:61:27 have lower hardness (16–20 GPa) than those with oxide weight ratio Al_2O_3:Y_2O_3:MgO = 42:44:14, which attained hardness values from 22 to 26 GPa.

During hardness examination the relationship has been noted between the values of hardness measured, degree of sintering and the amount of oxide precipitates. The higher the sintering degree, the higher both Vickers and Knoop hardness values. The larger

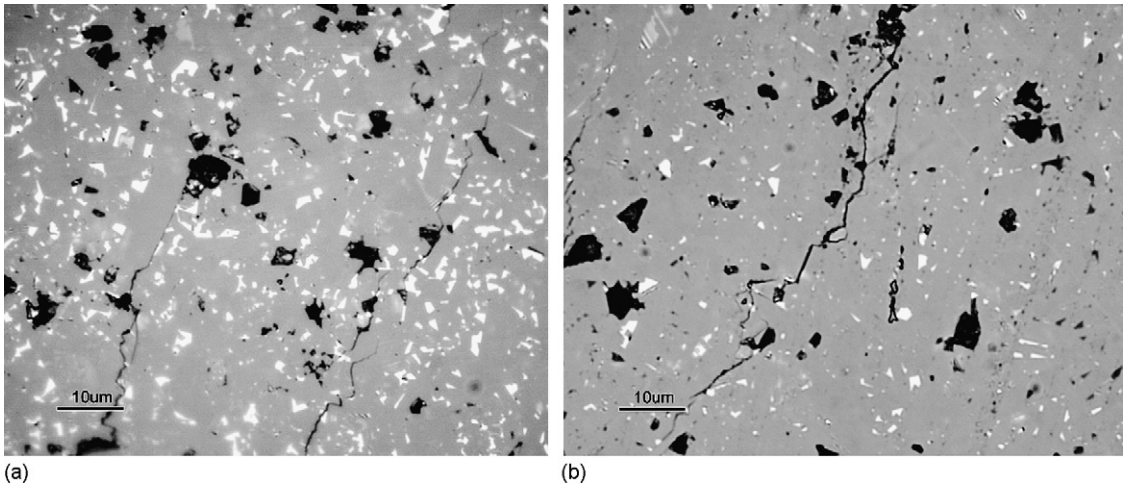

Fig. 10. Other features increasing fracture toughness: (a) extension and fragmentation of fracture path and (b) crack branching and networking.

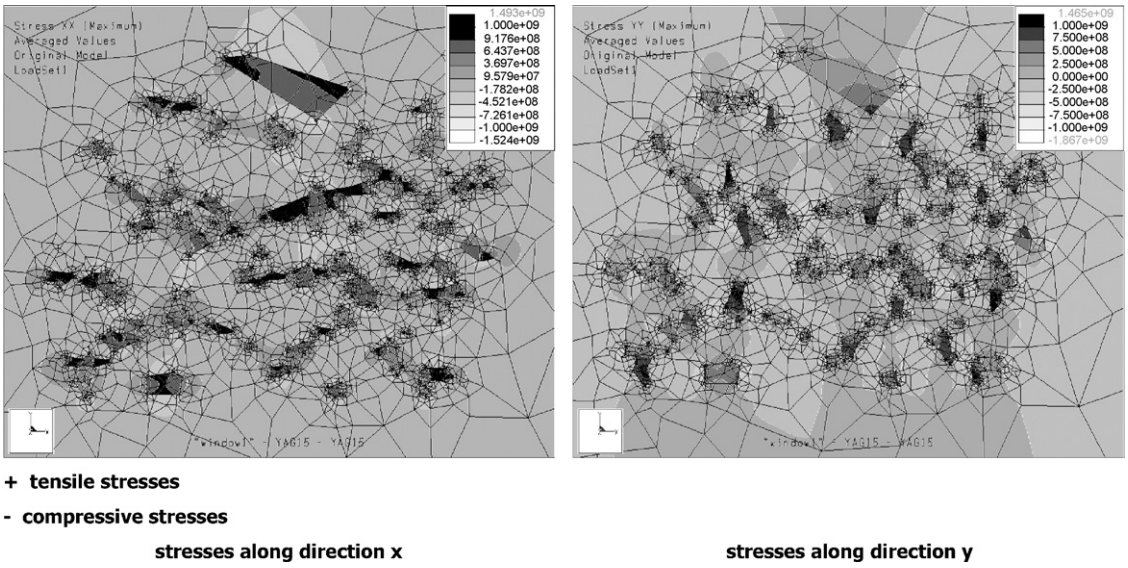

Fig. 11. Simulation of state of stresses in the examined materials.

the amount of oxide phases precipitates, the lower he hardness values.

The values of measured three-point bending strength of all examined materials remain within the limits ranging from 300 to 500 MPa (Table 3). The highest values, close to 0.5 GPa, are achieved by materials with significant mass contribution of oxide activators. The lowest values (~0.3 GPa), are typical of materials with lowest density (5% of 60% Al_2O_3 + 40% Y_2O_3 and 10% of 12% Al_2O_3 + 61% Y_2O_3 + 27% MgO), where the most significant stress concentration occurs on defects (pores), as it can be expected.

The fracture toughness, expressed as critical stress intensity factor K_{Ic} is relatively high for SiC materials and it is of the order of 5–6 MPa $m^{0.5}$. It is about 20–30% higher than values of fracture toughness measured on monophase SiC sinters with densification activated by small additions of carbon and boron. Increase of fracture toughness in the case of ceramic materials is most often achieved by change in the mode of crack propagation, when the effective fracture energy increase may occur. In the case of described here materials the precipitates of oxide phase appear within the SiC matrix. It may be easily observed that purposely initiated cracks propagate mostly along intergranular and interphase boundaries (Fig. 9b), whereas in monophase materials the cracks propagate in cross-granular mode (Fig. 9a). The fracture path is therefore significantly extended in polyphase sinters. The presence of precipitates of oxide phases develops stress fields within the SiC matrix due to important differences of the coefficients of thermal expansion of SiC ($\alpha \approx 4 \times 10^{-6}$ 1/deg) and oxide phase precipitates ($\alpha \approx 7 - 9 \times 10^{-6}$ 1/deg). Stress fields simulations performed for these materials using the Pro/Mechanica software (Fig. 11) indicate the presence of both, compressive and tensile, stress fields. Tensile stresses appear within the grains of the oxide phases precipitates while compressive stresses prevail within the SiC matrix (grains of SiC), and these are tangent to grain–matrix interface. Such stresses may cause increase of fracture energy due to hindering the crack propagation, which results in increase of the resistance to brittle fracture of this material. Crack branching, fragmentation and networking (Fig. 10) were observed within the examined SiC materials the sintering of which was oxide activated. All above mentioned phenomena may lead to increase of the effective fracture energy, which in turn brings about the increase of the resistance to brittle fracture of the discussed materials.

5. Summary

- The studies and their results presented here confirm the possibility of obtaining dense SiC materials by means of pressureless sintering, using oxide activators from the systems Al_2O_3–Y_2O_3 and Al_2O_3–Y_2O_3–MgO. In order to achieve high degree of densification it is necessary to prepare highly homogenous initial mixtures.
- Materials obtained through activated sintering are of polyphase nature. The precipitates of crystalline phases, like YAG, YAM, spinel and free Al_2O_3 have been identified within the SiC matrix.
- Microscopic observations allow to present the hypothesis that obtaining dense sinters is possible due to the presence of phases activating mechanisms of mass transport, thus facilitating densification process during sintering.
- From all examined materials the best properties and the highest densities are obtained using the following activators:

  - 10–15% $Al_2O_3 + Y_2O_3$ with weight ratio Al_2O_3:Y_2O_3 = 60:40;
  - 15–20% $Al_2O_3 + Y_2O_3$ with weight ratio Al_2O_3:Y_2O_3 = 40:60;
  - 10% $Al_2O_3 + Y_2O_3$ + MgO with weight ratio Al_2O_3:Y_2O_3:MgO = 42:44:14.

Acknowledgement

The present work was supported by The Ministry of Science and Information Society Technologies under grant no. 3 T08A 052 27.

References

1. Bloor, D. *et al.* ed., *The Encyclopedia of Advanced Materials, Silicon Carbide*, *vol. 1*. Elsevier Science Ltd., Cambridge, 1994.
2. Prochazka, S. and Scanlan, R. M., Effect of boron and carbon on sintering of SiC. *J. Am. Ceram. Soc.*, 1975, **58**(1/2), 72.
3. Suzuki, K., Ono, T., Shinohara, N., Dense sintered silicon carbide ceramics, US Patent 4354991 (1982).
4. She, I. H. and Ueno, K., Effect of additive content on liquid-phase sintering on silicon carbide ceramics. *Mater. Res. Bull.*, 1999, **34**(10/11), 1629–1636.
5. Sciti, D. and Bellosi, A., Effect of additives on densification, microstructure and properties of liquid-phase sintered silicon carbide. *J. Mater. Sci.*, 2000, **38**, 3849–3855.
6. Zhau, G. D., Mitomo, M., Sato, H. and Kim, Y. W., Fabrication and mechanical properties of fine-grained silicon carbide ceramics. *Key Eng. Mater.*, 1999, **161–163**, 243–246.
7. Cutler, R. A., Ikar, A. V., Hurford, A. C., Liquid phase sintering of silicon carbide, US Patent 4829027 (1989).